Numerical Simulations of a Subsonic/Supersonic Coaxial Jet for an Efficient Design of Experimental Setup

D. Guariglia*[1], C. Schram[1]

[1]von Karman Institute for Fluid Dynamics
*Corresponding author: Chaussée de Waterloo 72, 1640 Rhode-St-Genese, Belgium. daniel.guariglia@vki.ac.be

Abstract: The flow field of a coaxial jet with the internal (primary) flow being subsonic and the external (secondary) flow being supersonic has been investigated with COMSOL Multiphysics. We used the results to correct defects in the nozzle geometry and we evaluated the effect of heat transfer on the shock-cells system. Finally, we verified the stresses in the material to avoid permanent deformations in the nozzle. The simulations will be used to design efficiently the experimental setup for aeroacoustic and optical measurements.

Keywords: coaxial jet, supersonic, shock-cells, aeroacoustics.

1. Introduction

An efficient design of a new experimental facility in fluid dynamics requires always an iterative procedure and several steps must be followed, if we want to obtain the maximum number of benefits, at the minimum cost. One of these steps is the feasibility study, which can be done using a commercial software like COMSOL Multiphysics, which gives the possibility to explore the problem from different point of view, with consistent time savings.

This project is part of AeroTraNet2 Initial Training Network, a Marie Curie Actions with the aim to study the noise generated by a coaxial jet with inner flow being subsonic and the outer flow being supersonic in under-expanded conditions. This particular configuration leads to the formation of shock-cells between the inner and the outer shear layer which generate tonal and broadband noise (Fig.1). These are both an issue for the environment and a cause of fatigue stress for aeronautic structures.

At the von Karman Institute, a specific facility will be realized to simulate the shock-cells on a coaxial jet. We used COMSOL to verify the nozzle geometry and to have an insight of the flow field at various test conditions. This will help us in the definition of the experimental techniques that will be applied to the facility. Because of the limited computational power, we limited the simulations to have a sufficiently fine accuracy for designing purpose, not to study in detail the flow field. This will be done in future by the partners in the AeroTraNet2 network.

We used the **CFD interface** to have reliable prediction on the topology of the flow. The results will be used to design the experimental measurements setup, which will include aeroacoustic and optical instruments. We tested several pressure ratio configurations in order to define the most interesting ones to be investigated.

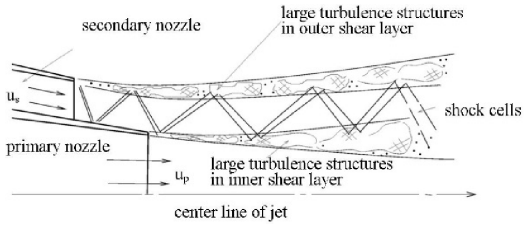

Figure 1. Sketch of shock-cells formation on a coaxial jet [4].

Then, we coupled the fluid dynamic problem with the **Heat Transfer in Solids** component with the aim to verify possible influences of the heat transfer through the nozzle walls itself on the boundary layer development, which is an important factor in the shock-cells noise formation. This could also lead to a more appropriate choice for the nozzle material.

Another important parameter in the nozzle design is the lip thickness of the nozzle. In the literature this parameter has been related to the formation of screech noise [1] [2] [3], that we would like to avoid in our setup. In order to do this, the lip thickness should be as thin as possible (fractions of millimeters). To verify that, we will not have excessive deformations in the nozzle lips due to the combined stresses of the shear stress, pressure and thermal stress, we used of the **Solid Mechanics** interface to compute them.

2. Geometric Model

The geometry is 2D axial symmetric. This gave us a substantial advantage in terms of computational time, which has been used to compute more refined meshes. The dimension of the nozzle are summarized in Fig 2. The external nozzle will be jointed to an already existent pipe of Ø = 30 cm (11.8 in); it has been created using a 3rd order polynomial spline. The inner nozzle has a simple conical shape and it will be jointed to an inner pipe of Ø = 9 cm (3.5 in). The nozzle exit areas dimensions are A_1 = 4.30e-4 m^2, A_2 = 14.41e-4 m^2, A_2/A_1 = 3.35.

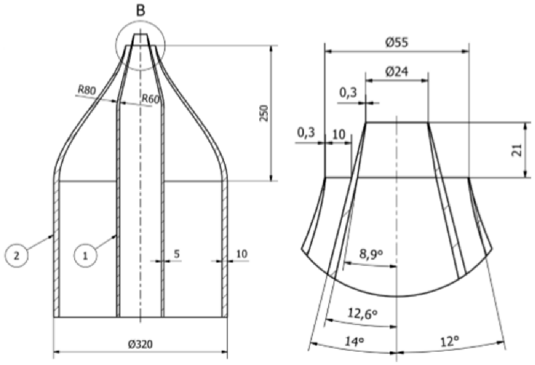

Figure 2. Dimensions of the coaxial nozzle [mm].

The final geometry has been obtained after that preliminary computations showed an incorrect position of the sonic throat in the external nozzle. Some small adjustments had been manually added to the inner profile of the secondary nozzle to fix the problem.

3. Fluid Dynamics Model

The simulation of the coaxial flow has been carried out by means of the interface "High Mach Number Flow", "k-ε model", from "Fluid Flow". Models "Fluid Properties and "Initial Values" are the default models included; they specified properties of air and initial velocities, correspondingly. In Fig.3 the geometry model and the initial conditions is depicted. Ambient pressure was taken to be p_a = 101325 Pa and the initial temperature was set to 293.15 K. We selected three boundaries "Inlet" at the bottom of the domain, two boundaries inside the nozzles (p_{01}, p_{02}, T_{01}=T_{02}= 293.15 K, M_1=M_2= 0.01) and the third outside (p_3 = 101325 Pa, T_3 = 293.15 K, M_3 = 0.01). The "Outlet" boundaries are the side and top edge of the domain with $p_{a,outlet}$ = 101325 Pa. The default model "Wall", "no slip", was applied to all surfaces of the nozzle.

We carried out many simulations varying only the total pressure of the two nozzle inlets. The test conditions are summarized in Tab.1.

Test ID #	CNPR	FNPR	$\dot{m}_1$ [Kg/s]	$\dot{m}_2$ [Kg/s]	BPR
1	1.675	2.45	0.171	0.845	4.95
2	1.72	2.5	0.176	0.862	4.90
3	1.645	2.425	0.167	0.836	5.01
4	1.626	2.4	0.164	0.827	5.03
5	1.589	2.35	0.160	0.810	5.07
6	1.518	2.25	0.150	0.776	5.17
7	1.45	2.15	0.140	0.741	5.28
8	1.385	2.05	0.130	0.707	5.43
9	1.353	2	0.125	0.689	5.53
10	1.235	1.8	0.102	0.621	6.07

Table 1. Test conditions for the simulations. Core Nozzle Pressure Ratio CNPR = p_{01}/p_a, Fan Nozzle Pressure Ratio FNPR = p_{02}/p_a, theoretical mass flow m_1, m_2, Bypass Ratio BPR = m_2/m_1.

3.1 Initialization

Often, one of the major problems of numerical simulation is the initialization. This could require time dependent computation where the imposed condition at the inlet change in time to smoothly arrive at the target ones. In our configuration, with the presence of a chocked section, we found as well that was impossible to initialize the computation starting with the defined inlet conditions and zero velocity in all the domain. However, instead of running time dependent simulation, we managed to initialize the code by simply imposing velocities and pressures at specified subdomains, guessing the behavior of the fluid when stationary as shown in Fig.3.

To reduce times, we decided to use these initial conditions for the test ID 1 only. For the other test IDs, we used the results of precedent computation, changing only the "Inlet" boundaries.

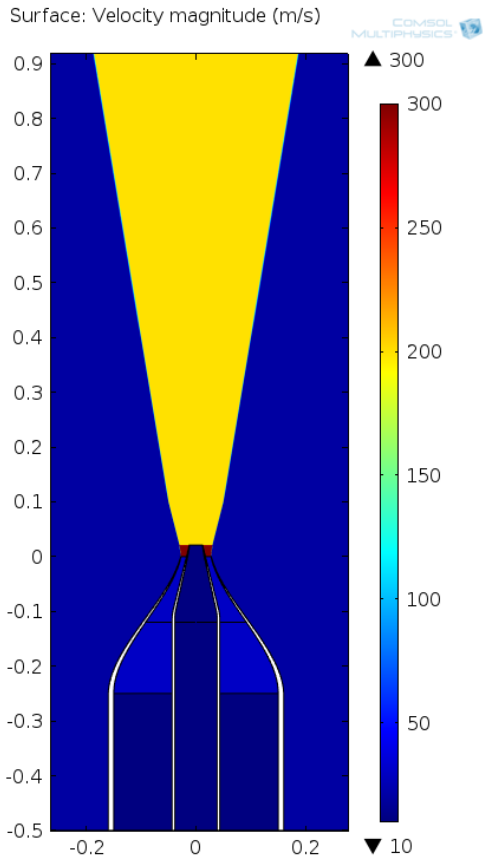

Figure 3. Simulation domain with initial condition for the velocity.

4. Thermal Model

The Heat Transfer in Solids Interface is a component of the CFD module, this easily consented us to run a coupled simulation simply adding this interface to the "Physics". The reason to go for this is because we expect a heat transfer through the thin walls of the nozzle. In particular from the internal flow (warmer) to the external one (colder). Knowing that a positive heat flux has destabilizing effects on the boundary layer, we wonder if this could affect the developing of the supersonic region (in particular the position of the first shock), and so, the whole shock-cells pattern.

We selected from the COMSOL material library two materials currently in use at VKI for manufacturing, brass and steel. These have significantly different thermal conductivity as well Young's module and yielding stress. As boundary conditions we simply imposed a fixed temperature, $T_m = 293.15$ K, at the bottom edge of the nozzles, then we set the same as initial temperature inside the material.

5. Structural Model

The simplest way to couple CFD problems with structural problems would have been to use the **Fluid-Structure Interface**. This option was unfortunately not available for our license, so, we had to split the problem and run the CFD and structure mechanics separately.

As boundary conditions, we simply imposed the "Fixed Constraints" to the bottom edge of the nozzle, leaving the other boundaries as "Free". The remaining part was to set the load conditions to the structure. In the various options, figured the pressure on the boundaries, that we could impose manually for each boundary. The simplest thing to do would have been to impose a fixed pressure to the inner side of the nozzle and the ambient pressure on the outer side. This, however, would have been unphysical, because the internal pressure is changing (in this case decreasing) along the nozzle length. We decided so, to use a function as boundary load condition with the pressure extracted from the CFD results.

In "Global Definitions" we created an "Interpolation Function, Bund_Load", where we loaded the text file containing the pressure on the walls extracted from the CFD results. Finally, we set up the "Boundary Load" inserting the function Bund_Load(r,z) in the pressure field.

6. Meshes

We started with the built-in "Physics Controlled Mesh" and the "Extremely fine" option, so, the program created free triangles and boundary layer elements on the walls. This option, however, led to have an unnecessary high number of points outside the nozzle. For this, we switched to the "User-defined" settings, and we discretized the subdomains independently. After some results, we realized that it was not sufficiently fine in the supersonic region, so we created two other meshes with higher resolution and we tested on the same conditions. An example of the Mesh 1 and Mesh 2 in the nozzles exit region is shown in Fig.4. Mesh 3 has the minimum size being the half of Mesh 2 and it has been

omitted for clarity. Details on the three meshes are shown in Tab.2.

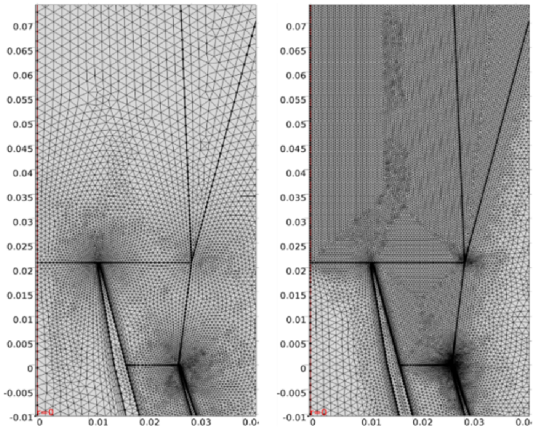

Figure 4. Comparison of "Physics Controlled" Mesh 1 and "User-defined" Mesh 2. The red line corresponds to the location where the Mach number has been evaluated to compare the meshes.

	Maximum element size in the shock region	Number of elements
Mesh 1	0.002	3.4×10^5
Mesh 2	0.0005	2.7×10^5
Mesh 3	0.00025	6.0×10^5

Table 2. Main characteristics of meshes used for comparison

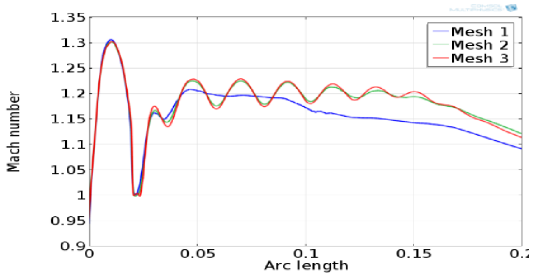

Figure 5. Comparison of "Physics Controlled" Mesh 1 and "User-defined" Mesh 2 and Mesh 3. Data has been extracted from the dashed line in Fig.6

The comparison between the three meshes has been done plotting the Mach number along a line starting at the beginning of the supersonic region. The graph in Fig.5 shows how the results for Mesh 1 has poor resolution in comparison of Mesh 2 and Mesh 3. The Mesh 2 is capable to calculate the first peak in amplitude and location, then for the other peaks the location is predicted accordingly with Mesh 3, but the amplitude is slightly different. In conclusion, because of the relatively high computational cost of Mesh 3, we decided to make all the simulations using the Mesh 2.

7. Results

The flow field appears to be quite complex and it changes significantly varying the pressure conditions. At higher pressure, we can observe the formation of a first supersonic cell, which is interrupted by an oblique strong shock wave starting at the lip of the internal nozzle (Fig.6). After that, the external flow became again supersonic and have the formation of shock-cells in the wake, between the internal shear layer and the external shear layer.

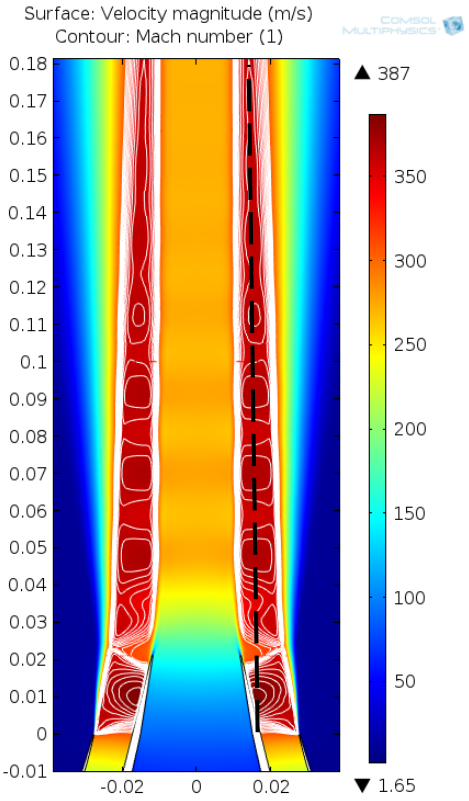

Figure 6. Velocity flow field of test ID #1. The contour plot shows the regions with Mach > 1. It is possible to recognize the shock-cells in the wake. The black dashed line corresponds to the chosen location where data is extracted for comparison.

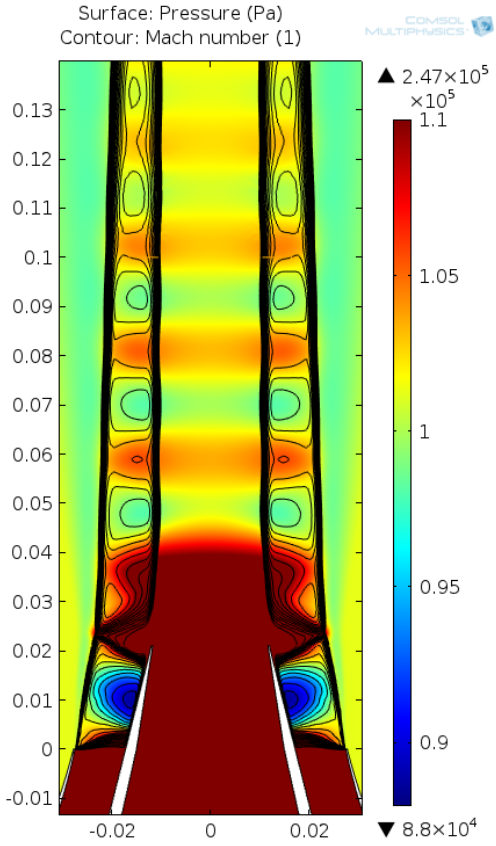

Figure 7. Pressure flow field of test ID #1.

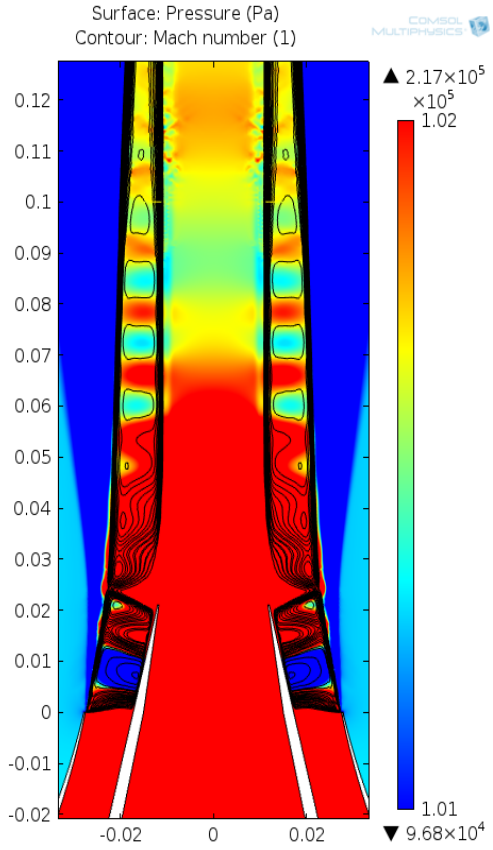

Figure 8. Pressure flow field of test ID #7

Reducing the total pressure we can observe a progressive reduction on the length of the shock-cells. It is worthy to note that pressure in the wake is oscillating accordingly with the shock-cells and it is transmitted from the supersonic to the subsonic region. From an aeroacoustic point of view, the length of the shock-cells could be related to the broadband noise frequency peak. According to Tam *et al* [4] we have a pressure wave emission each time a turbulent structure passes a shock-cell. This means that lowering the pressure we should expect in the experiments higher broadband noise frequencies, because the wavelength is reducing.

Lowering the pressure, we arrive to another flow regime. In Fig.8 we can recognize the formation of shock-cells both in the wake and in the region between the external shear layer and the wall of the internal nozzle. This could have a negative effect on the aeroacoustic point of view. Because the length of the two kind of shock-cells are different, we should expect the appearance of other broadband or tonal noise.

Lowering further the total pressure, we assist at the disappearance of the shock-cells in the wake, while they are still present in the region immediately after the secondary nozzle (Fig.9).

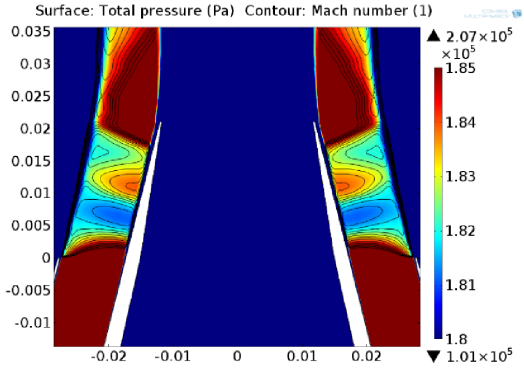

Figure 9. Pressure flow field of test ID #8.

Finally, we can compare all the test conditions in a unique plot where we can appreciate the differences. In particular, in Fig.10 we can

observe the fluid transition into the three flow regimes described above.

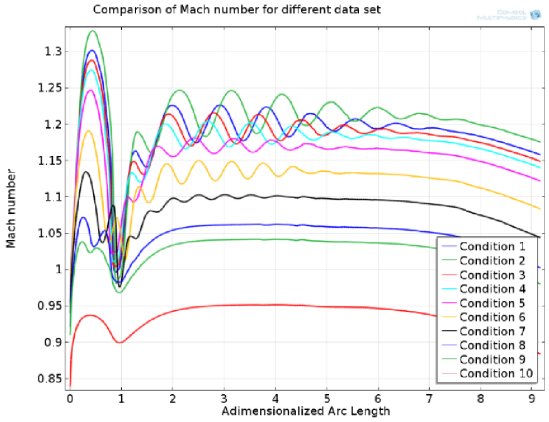

Figure 10. Comparison of Mach number of all test IDs along a line described in Fig.6. The x axis has been adimensionalized by the primary nozzle diameter

From the point of view of the mass flow rate, we can find important differences from the theoretical values (Tab.2). We can find two explanation for this behavior: when the external flow is supersonic, we have a strong shock at the end of the primary nozzle. The strong recompression affect the primary flow too, and this cause the minor mass flow rate, because the nozzle is not adapted to ambient pressure.

	mass flow COMSOL		**Difference in percentage**	
Test ID #	$\dot{m}_1$ [Kg/s]	$\dot{m}_2$ [Kg/s]	**diff_$\dot{m}_1$ %**	**diff_$\dot{m}_2$ %**
1	0.118	0.817	-31.9	-4.9
2	0.121	0.834	-32.1	-4.9
3	0.115	0.809	-32.1	-4.9
4	0.114	0.801	-31.9	-4.9
5	0.111	0.784	-31.6	-5.0
6	0.104	0.750	-31.9	-5.0
7	0.091	0.716	-36.5	-5.1
8	0.082	0.681	-38.4	-5.3
9	0.077	0.664	-39.3	-5.4
10	0.058	0.591	-44.7	-6.4

Table 2. Mass flow rate comparison between the theoretical values of Tab.1 and those calculates with COMSOL.

When the flow is, instead, completely subsonic, as for test ID 10, we have a shielding effect of the secondary flow. It happens that the secondary flow is adapted to ambient pressure, but it is still faster than the primary one. At the end of the primary nozzle, the two flows mix in the shear layer; this cause to the secondary flow to slow down, and contemporary to increase its pressure. This is transmitted to the inner flow which as reaction reduces its mass flow rate, so the primary velocity slow down more, and the same for the secondary flow velocity in the shear layer, with a consequent increase in pressure, and so on. This until an equilibrium is reached.

7.1 Aeroacoustic content

We used the data to estimate the range of frequencies that we should expect to observe during the experiment. As rule of thumb, we calculated the time that a vortex, generated at the lip of the external nozzle and being convected by the flow, would take to cross a shock-cell. To do this, we extracted data from a streamline and we computed the travel time to cross the first shock-cell in the wake (starting after the strong shock). The results for all the test ID are plotted in Fig. 11. As stated previously, we expect an increase of frequency as consequence of the shortening of the shock-cells. Interesting is the case of test ID 2, where the frequency is higher than test ID 1, despite higher total pressure. This happened because the increase of the average velocity was more important than the increase of the shock-cell amplitude. For test ID 7 we can calculate two frequencies, one for the shock-cells in the wake, and the other one for those at the secondary nozzle exit.

Of course, this relationship has to be verified experimentally, but nevertheless it can give useful information for the experimental setup. In terms of microphones, we know now that we should go for high frequency response sensors, to be able to capture correctly the noise. In terms of optical setup for PIV techniques, knowing the velocities we can determine from the beginning a good sized interrogation area, as well as the timing for the acquisition.

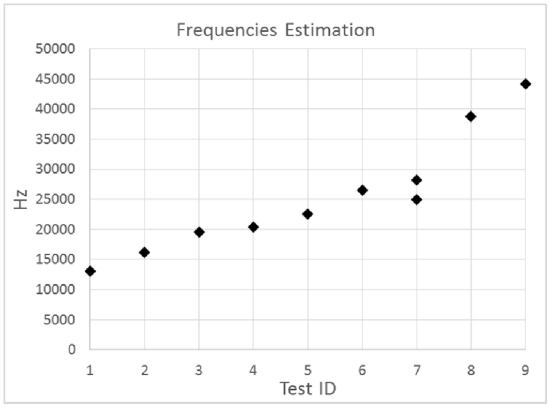

Figure 11. Frequency range estimation for all test conditions.

7.1 Thermal model results

We ran simulations with and without considering the heat flux through the wall. Results showed how both with steel and brass, despite being good conductors, the temperature difference is not sufficient to influence the shock-cells pattern. To verify this, we tried to increase the total temperature in the primary flow up to T_{0p} = 1000 K; in this case we could notice some differences in the position of the first shock-wave. This convinced us that heat transfer play a very little role in this experiment.

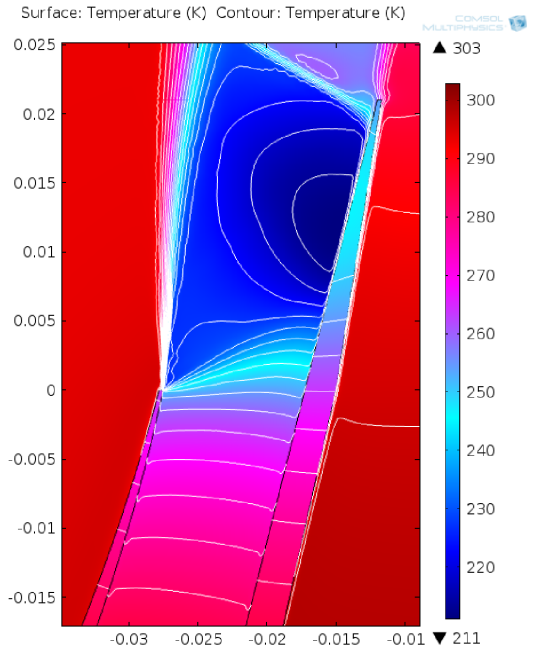

Figure 12. Temperature map with temperature isolines of test ID 1.

7.2 Structural model results

In Fig.13 we can see the results of the simulation for test ID 2 in case of brass. The maximum von Mises stress is well below the yielding point of the material, despite the small thickness of the lip edge. The displacements as well (magnified 14000 times in the figure), are negligible.

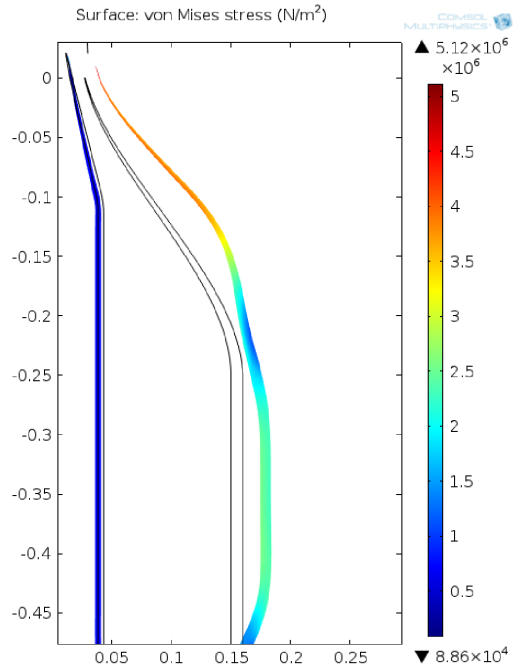

Figure 13. von Mises stresses and displacements magnified 14000 times for test ID 2.

8. Conclusions

We conducted simulations of a subsonic/supersonic coaxial nozzle for various inlet conditions, coupling the CFD with the heat transfer problem through the walls and we used those results as input for the structural problem. We verified that heat transfer plays a negligible role in the shock-cells development, and that the nozzles are well dimensioned. We observed very interesting flow behavior, which will be investigated experimentally in the future and compared with the computational results.

9. References

1. Powell, A.,"On the Mechanism of Choked Jet Noise," Proceedings of the Physical Society of London, Vol. 66, No. 408, 1953,pp. 1039–1056)

2. Raman, G.,"Supersonic Jet Screech: Half-Century from Powell to the Present," Journal of Sound and Vibration, Vol. 225, No. 3, 1999, pp. 543–571.

3. Tam, C. K. W., Seiner, J. M., and Yu, J. C., "Proposed Relationship Between Broadband shock Associated Noise and Screech Tones" Journal of Sound and Vibration, Vol. 110, No. 2, 1986, pp. 309–321

4. Tam, C. K. W., Pastouchenko, N. and Viswanathan K., "Broadband Shock-Cell Noise from Dual Stream Jets" 14th AIAA/CEAS Aeroacoustics Conference (29th AIAA Aeroacoustics Conference). May 2008

5. André, B., Castelain, T., and Bailly, C., "Broadband Shock-Associated Noise in Screeching and Non-Screeching Underexpanded Supersonic Jets", AIAA Journal, Vol. 51, No. 3 2013, pp. 665-673.

6. Viswanathan, K., "Instrumentation Considerations for Accurate Jet Noise Measurements", AIAA Journal, AIAA Journal, American Institute of Aeronautics and Astronautics, 2006, 44, 1137-1149

7. Jeronimo, A., "Application of PIV to a Supersonic Jet", Technical Report, von Karman Institute, 2001

8. Kiran, A., "Jet noise : aeroacoustic distribution of a subsonic co-axial jet". PhD thesis, University of Warwick, 2008.

9. Bhat, T., Ganz, U., and Guthrie A., "Acoustic and Flow-Field Characteristics of Shock-cell Noise from Dual Flow Nozzles" 11th AIAA/CEAS Aeroacoustics Conference. May 2005